'undercompaction' or 'compaction disequilibrium', of PP generation during deposition is different from fluid expansion mechanisms of PP generation, as these mechanisms occur at a later age than deposition. Fluid expansion mechanisms - hydrocarbon maturation, aquathermal expansion and mineral diagenesis, fall in Type II PP generation mechanisms (Bowers 1994) and generated overpressure is a result of pore fluid trying to expand inside counteractive rock-matrix constraining expansion. Due to higher rate of PP increase than the overburden stress unlike the undercompaction, these mechanisms are not readily detectable using seismic velocities (Tingay et al. 2009).

Stress relationship between effective stress (stress acting on grain-to-grain contacts) and PP (Terzaghi 1929 and 1943), finds a useful application as seismic wave velocity can be related to effective stress, which in turn can be inverted to estimate PP. During normal compaction, seismic velocity (elastic wave velocity) increases with depth as porosity reduces and grain-to-grain contact increases. During undercompaction the effective stress freezes in time rather than decreasing and velocity maintains its past maximum value, hence, porosity vs. velocity curve lies on a loading curve, whereas during fluid expansion mechanisms effective stress decreases with a velocity reversal and porosity vs. velocity curve lies on an unloading curve (Tingay et al. 2009 and 2011, **Fig 2 (a)**).

As we discuss further in detail in this paper, predrill PP prediction is critical as stated above, but what made the whole process of executing planned drilling operations safe and successful has been real-time PP monitoring and detailed post-drill PP analysis based on the data acquired during and/or after drilling operations to identify PP type and its generation mechanism.

Geological Understanding

The study area belongs to the shallow-to-deep offshore of East Coast of India. The basin, a pericratonic onshore basin extending offshore beyond the midslope along the eastern continental margin of India, has been mainly fed by the river systems and numerous tributaries. The depositional setting comprises of a well-defined shelf, slope and deepwater system (Rao 2001), **Fig 1(a)** and **Fig 1(b)).**

The offshore basin's characteristic feature is its en-echelon horst and graben system which is filled with a thick pile of sediments of Permian-to-Recent age. Basin's formation is credited to the rifting along the eastern continental margin in early Mesozoic. Formation of the series of horst and grabens cascading down towards the ocean led to different reservoir compartments separated by steeply dipping faults. In the Tertiary, the area became structurally deformed by numerous sets of growth faults and released fractures (Gupta 2006). In deltas as the sediment is loose and due to large sediment input into the basin and slope stability numerous growth faults develop. Due to the high sedimentation rate in deltas, initially present fluid cannot escape the pore spaces resulting in abnormally/over-pressured formations, in which formation pressure has been found to be twice as high as hydrostatic pressure.

Predrill Pore-pressure Modelling

Seismic velocities ('RMS' or 'Average') available from the planned well locations (**Fig 3(b)**) were analyzed and converted to Interval Seismic Velocity (Dix 1955). These acoustic velocities converted to interval velocities are driven by fundamental intrinsic properties of rock matrix, grains, pore spaces, and the pore fluid properties. Resolution or coarseness of the seismic velocity points varied from one to another based on variation of seismic data acquisition and processing methodologies for planned well locations.

Offset wells for these four planned exploratory wells, in deepwater water environment, from near-by blocks were used for postdrill analyses prior to predrill PP prediction. Petrophysical log data was used to develop postdrill PP and FG models, which were calibrated with field acquired measurements and drilling events. Estimation of overburden was done using available density log, and acoustic velocity to density transform (Gardner 1974) was carried out to estimate or correct density data wherever density data was missing or incorrect. As there is substantial difference in water depths of all four planned wells, different set of offset wells were used for each of planned locations. The consideration of difference in water depths is critical as mud line density decides the profile of overburden density, especially when shallow overburden has different consolidation rate based on overlying water column.

Eaton's method (Eaton 1975) based on resistivity and acoustic velocity data was used for PP modelling using the similar compaction trends to that of the offset wells. This in-depth analysis to understand PP

A Close-the-Loop well delivery of deep-water exploratory wells, Krishna Godavari Offshore, East Coast of India

regimes' dependency on stratigraphy and structure helped in understanding shale pressure evolution and sand-shale pressure relationship for the prevalent PP with respect to the regional geology. As it became evident with modelling of the offset wells for each of the planned locations, that more than the maximum value of the PP it was the top of ramp which varied significantly from one well to another and was critical to be ascertained during well planning stage itself. Available offset wells range over a time of more than couple of decades, and hence some of them have only limited field acquired pressure data available. The petrophysical log data used to model PP is useful for shale lithology but are not entirely useful for non-shaly lithologies such as carbonates. This analysis not only helped in identifying the major issues encountered while drilling the offset wells but also provided a detailed understating of PP profile and the range of depths of encountering top of ramp for each of the planned well locations.

The learnings from the offset wells' modelling analysis and direct pressure measurements available from these offset wells were used to develop the PP models for planned wells – Well A, Well B, Well C & Well D. PP profile modelled using seismic interval velocity data were interpreted and calibrated based on the direct pressure measurements – formation fluid pressure and leak-off tests. Driven by the variation in seismic velocity data at planned prospect locations, three possible PPFG scenarios were predicted for each prospect, and base-case was carried forward for well design and planning exercise (**Fig 4(a)**.

Realtime Monitoring

Owing to the expected potential issues while drilling these planned deep-water wells, a robust real-time monitoring set-up was established for each section of the well. Using the real-time streamed data – LWD data, MWD data and drilling parameters, PP monitoring was performed, and a robust communication and decision-making protocol helped to steer the wells to the planned targets.

Below is one of the examples of how critical the real-time monitoring and PP prediction during drilling operations has been, **Fig 4(b)**. Example is from Well C, while for majority of the borehole section PP followed predrill trend, it's near the Zone1-Zone2 transition where surprise was encountered.

The new section of the borehole, penetrating through Zone1-Zone2 transition, was started drilling with adequate overbalance based on the predrill PP trend, so high enough that the surprise, shallower than expected PP ramp, was already covered by the MW/ECD being maintained. From the middle of Zone2 onwards the further increase in PP was modelled in real-time which prompted further proactive increments in MW, prior to entering Zone3. The narrow drilling window was taken care of via effective hole cleaning measures to maintain ECD on the lower side while maintaining effective downhole mud-pressure. Near real-time analysis of hydraulics design and kick tolerance for upcoming borehole section(s) were used to further optimize the drilling mud design while maintaining bottom hole pressure.

The increase in TG% (Total gas%) near the middle of Zone3 further confirmed that the PP ramp was encountered shallower than the depth at which it was predicted, and pressure was still following an increasing trend even in Zone3. Formation pressure data (MDT points) acquired after drilling also confirmed the interpretation of PP made in real-time. There were numerous such instances which could not only have really challenged the safety of these wells and jeopardized the well targets but could also have resulted in increased operational cost and NPT.

Postdrill Analysis

Estimation of PP and FG was carried out for wells – Well A, Well B & Well C, using the acquired wireline log data (petrophysical logs – bulk density, resistivity & compressional sonic) and field pressure points (formation fluid pressure and formation fracture pressure, both), **Fig 5**. The comparison of predrill and postdrill PP trends show little variance (~0.25-0.50ppg) for both Well A and Well B, whereas for Well C encountering the pressure ramp shallower than anticipated resulted in pressure variance of up to ~0.75-1.0ppg at few depth points, but still the max pressure modeled during predrill and postdrill analysis show minor variation (~0.25ppg). This deviation in PP can possibly be due to the shallow penetration of high pressure sands of Zone 3, eventually leading to shallow pressure ramp.

Postdrill analysis shows that the reservoir sections in Zone 2 have variation in formation pressure (~1.5-2.0ppg), from location Well B to Well C. Whereas, Zone 1 has consistently shown a similar pressure trend for different well locations.

A Close-the-Loop well delivery of deep-water exploratory wells, Krishna Godavari Offshore, East Coast of India

The low variance in predrill and postdrill pressures for locations Well A and Well B can be attributed to similar velocity trends as interpreted from seismic and acquired compressional sonic slowness. While for location Well C, the predrill seismic velocity may have averaged out the response from high pressure shales as sonic interpreted velocity gives lower values in comparison to seismic velocity at the depth which show pressure variance.

The postdrill models and available wireline log data were used to further analyze the overpressure generation mechanism for all three drilled wells. Plotted compressional velocity data, estimated from wireline compressional slowness data after removing any abnormal/erroneous data points, against vertical effective stress [VES; VES = Overburden pressure (OBG) – PP], Bowers 1994. Thus, established trend falls on the loading curve of VES vs Compressional Velocity plot and indicates disequilibrium compaction to be the cause of overpressure generation. Furthermore, the compressional velocity against formation bulk density (clean and noise free formation bulk density data) signatures were analyzed to confirm the overpressure generation mechanism, Hoesni 2004 (**Fig 2(b)**). Even this set of data falls on the trends depicting disequilibrium compaction as the sole mechanism responsible for 'abnormal or overpressure generation' (**Fig 6**).

Conclusions

The close-the-loop study (**Fig 3(a)**) to develop models and to impart learnings into future wells has been immensely valuable and has helped gain incremental knowledge with every drilling campaign.

References

Bowers, G.L., 1994. PP estimation from velocity data: Accounting for overpressure mechanisms besides undercompaction. IADC/ SPE 27488, IADC/SPE Drilling Conference, p. 515-530.

Eaton, B.A., 1972. Graphical method predicts geopressured worldwide, World Oil, v 182: p51-56.

Gardner, G.H.F., Gardner, L.W., Gregory, A.R., 1974. Formation velocity and density – the diagnostic basis for stratigraphic traps. Geophysics 39 (6): p.770-780.

Gupta, S.K, 2006. Basin architecture and petroleum system of Krishna Godavari Basin, east coast of India, The Leading Edge, v25, no. 7: p 830-837.

Hoesni, M.J., Swarbrick, R.E, and Goulty, N.R 2003. The Origins of overpressure in the Malay Basin. AAPG Barcelona Conference, Spain, 2003.

Hottman, C.E., Johnson, R.K., 1965. Formation Pressure from Log-Derived Shale Properties, Paper (SPE1110) presented at 40th Annual SPE Meeting in Denver.

Khazanehdari, j., 1998. The effects of pore fluid pressure, confining pressure and pore fluid type on the acoustic properties of a suite of clean sandstones, 1998, American Association of Drilling Engineer Conference Paper.

Rao, G.N, 2001. Sedimentation, stratigraphy and petroleum potential of Krishna-Godavari basin, East Coast of India. AAPG Bulletin, v.85, no.9: 1623-1643.

Sayers, C.M., 2006. An introduction to velocity – based PP estimation, The Leading Edge, v 25, no. 12: p 1496-1500.

Tingay, M., Hillis, R., Swarbrick, R.E, Morley, C., and Damit, R., 2010. Origin of Overpressure and Pore Pressure Prediction in the Baram Delta Province, Brunei, March 2011.

Acknowledgments

The details described in this paper are a result of experience gathered by the staff of the RTOC Team, Mumbai, Oil and Natural Gas Corporation Ltd and Geomechanics team of Schlumberger Asia Services Limited. We would like to thank management of ONGC for their support and permission for publishing this paper.

A Close-the-Loop well delivery of deep-water exploratory wells, Krishna Godavari Offshore, East Coast of India

Figures

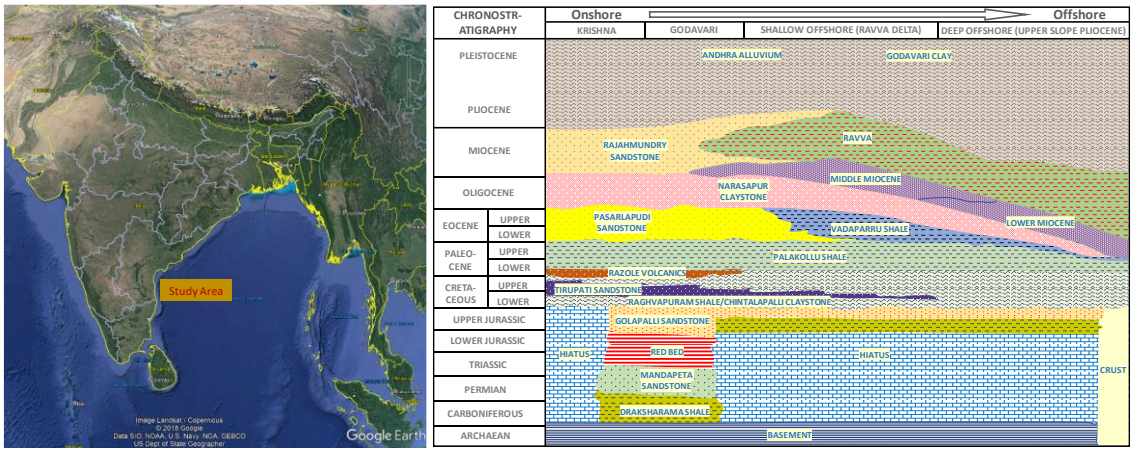

Fig 1(a): Location map of the study area; **(b)**: Schematic representation: Chrono stratigraphy - East Coast, India.

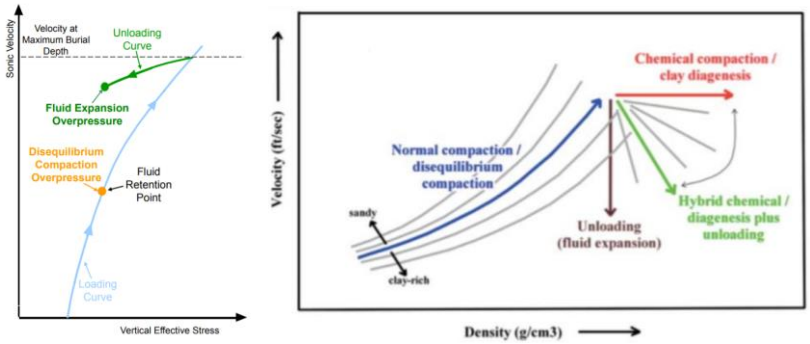

Fig 2 (a): Bower's plot: Effective vertical stress vs. compressional wave velocity (Tingay 2011); **(b)**: Hoesni plot: Bulk density vs. compressional wave velocity (Hoesni 2004).

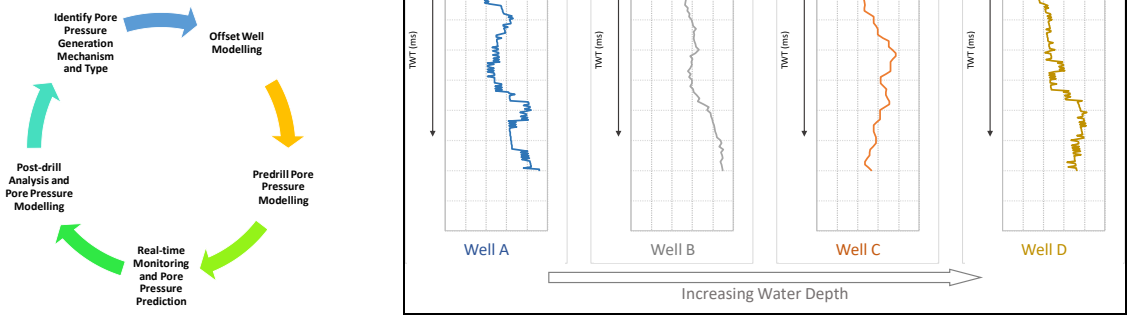

Fig 3(a): Adapted close-the-loop study cycle; **(b)**: Seismic velocities for all the four planned locations in increasing order of water depth.

A Close-the-Loop well delivery of deep-water exploratory wells, Krishna Godavari Offshore, East Coast of India

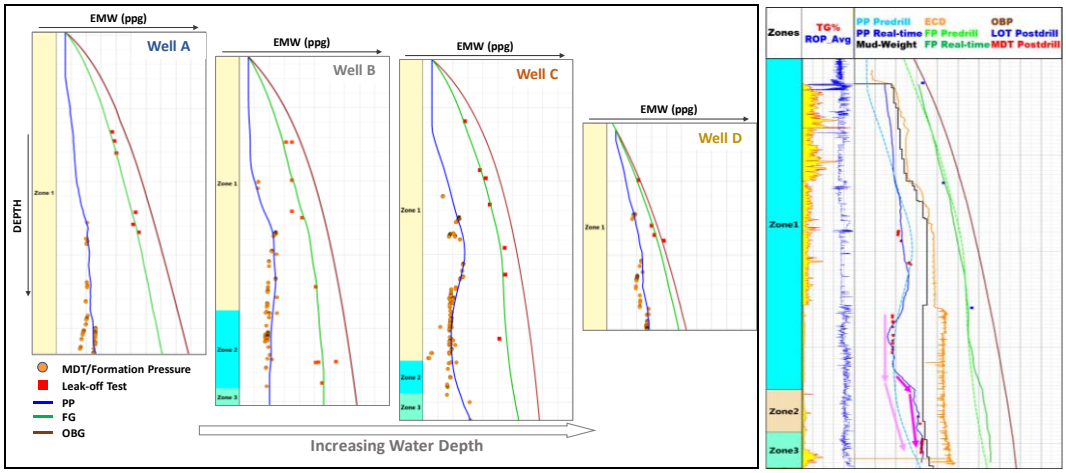

Fig 4(a): Predrill pore pressure and fracture gradient models for the four planned locations in increasing order of water depth; **(b)**: Real-time pore pressure – fracture gradient monitoring window for Well C.

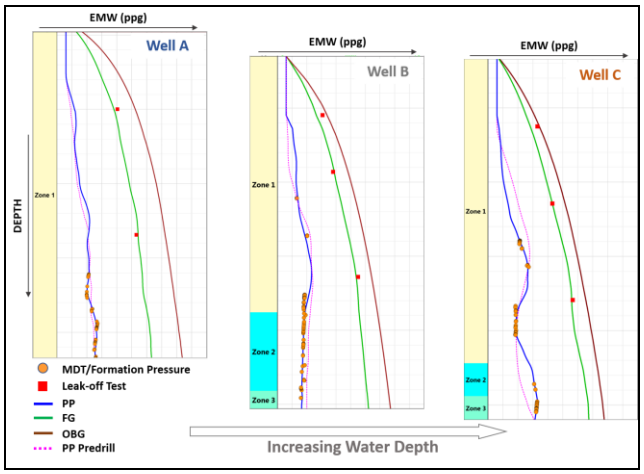

Fig 5: Postdrill pore pressure – fracture gradient models for the all three wells drilled till the time of this study.

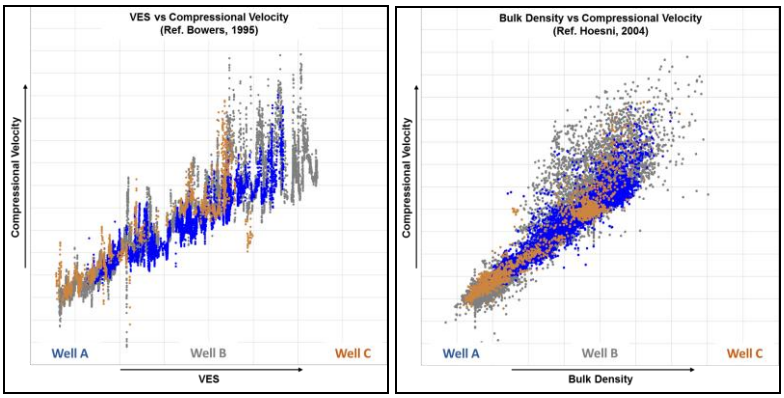

Fig 6: Bower's and Hoesni plots for Well A, Well B and Well C.